Supporting Information

From porous to dense Tm^{3+}-Lu_2O_3 micro- and nanosized crystalline morphologies designed through hydrothermal precursors: assessment on infrared emission properties

Concepción Cascales,* Carlos Zaldo, Fátima Esteban-Betegón and Rocío Calderón-Villajos

* (e-mail ccascales@icmm.csic.es)

Instituto de Ciencia de Materiales de Madrid, Consejo Superior de Investigaciones Científicas CSIC, c/Sor Juana Inés de la Cruz, 3, E-28049 Madrid, Spain.

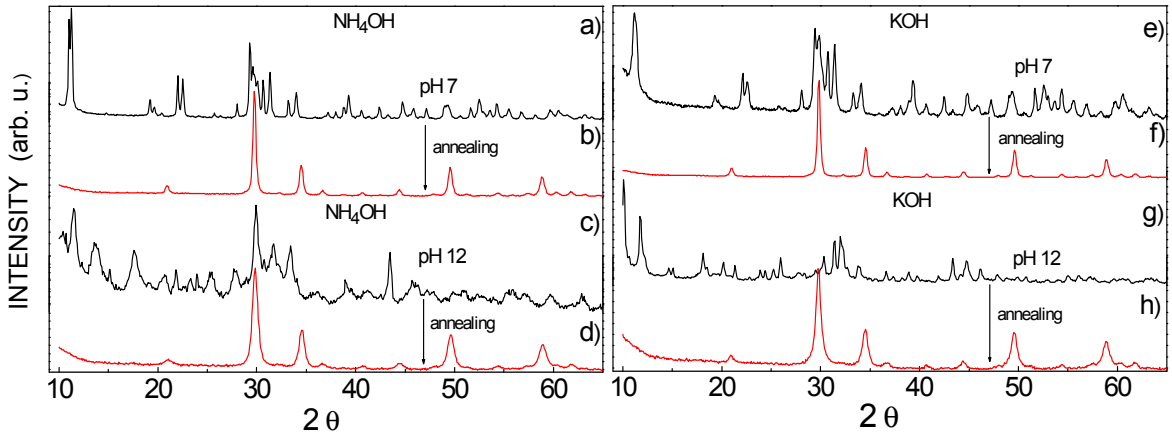

Figure ESI-1. X-ray diffraction patterns of products of hydrothermal syntheses by using Lu(Tm) nitrate (NIT) reagents: a) and c) hydrothermal precursors **P**-NIT1-A and **P**-NIT2-A; b) and d) $Lu_{1.99}Tm_{0.01}O_3$ **S**-NIT1-A and **S**-NIT2-A sesquioxides. e) and g) hydrothermal precursors **P**-NIT1-B and **P**-NIT2-B; f) and h) $Lu_{1.99}Tm_{0.01}O_3$ **S**-NIT1-B and **S**-NIT2-B sesquioxides.

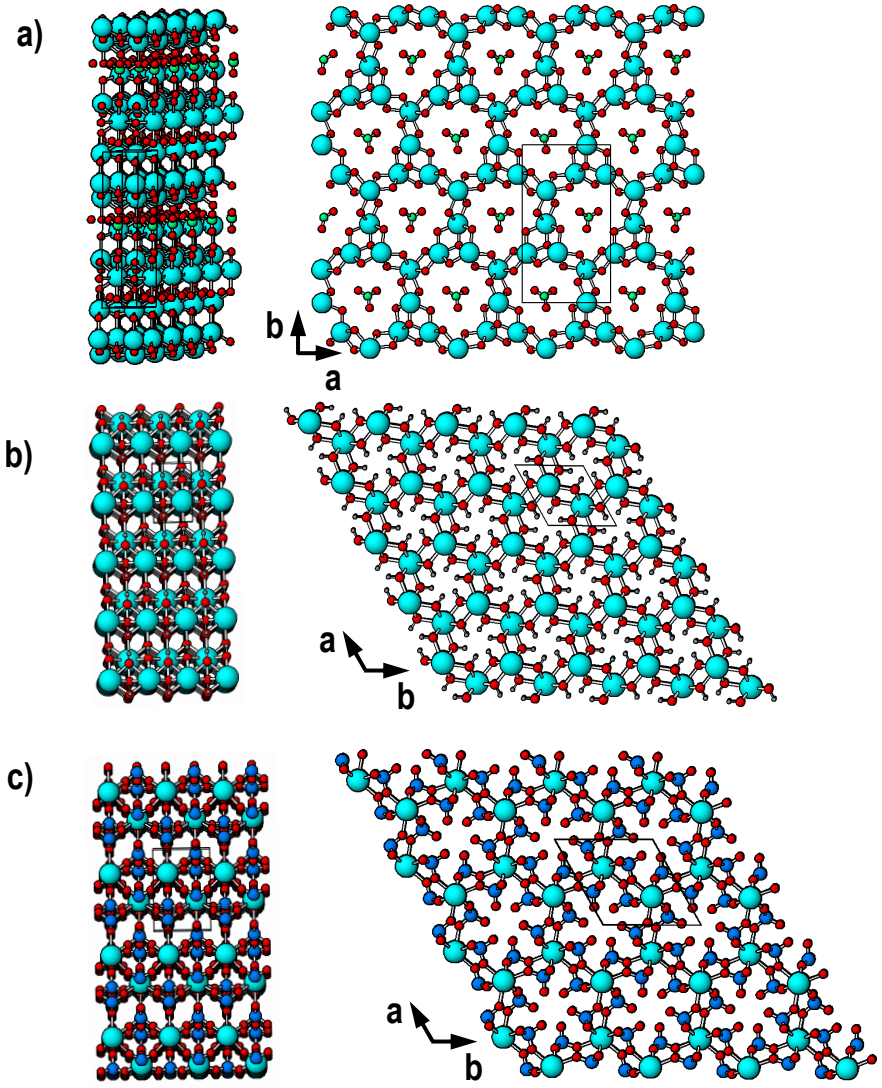

Figure ESI-2. Views of the quasi-layered structure of crystal phases present in prepared hydrothermal precursors: a) monoclinic $P2_1$ $Er_4O_2(OH)_8 \cdot HNO_3$, along the *c* axis (left), and in the *ab* plane (right), cyan, green and red balls for Er, N and O atoms, respectively; hexagonal $P6_3/m$ structures of b) $RE(OH)_3$ and c) $Er(ClO_4)_3$, along the *c* axis (left) and in the *ab* plane (right), cyan, red, grey and blue balls for Er, O, H and Cl atoms, respectively.

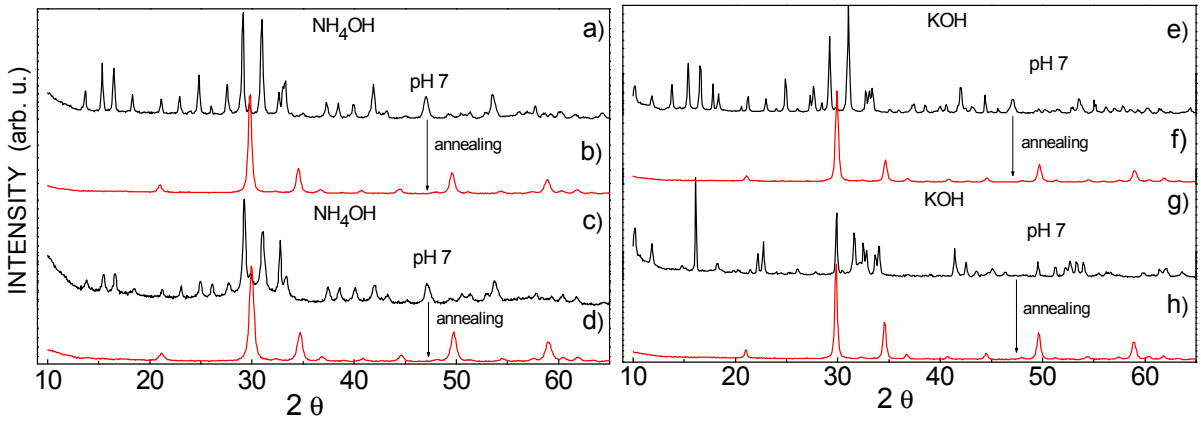

Figure ESI-3. X-ray diffraction patterns of products of hydrothermal syntheses by using Lu(Tm) chloride (CHL) reagents: a) and c) hydrothermal precursors **P**-CHL1-A and **P**-CHL2-A; b) and d) $Lu_{1.99}Tm_{0.01}O_3$ **S**-CHL1-A and **S**-CHL2-A sesquioxides. e) and g) hydrothermal precursors **P**-CHL1-B and P-CHL2-B; f) and h) $Lu_{1.99}Tm_{0.01}O_3$ **S**-CHL1-B and **S**-CHL2-B sesquioxides.

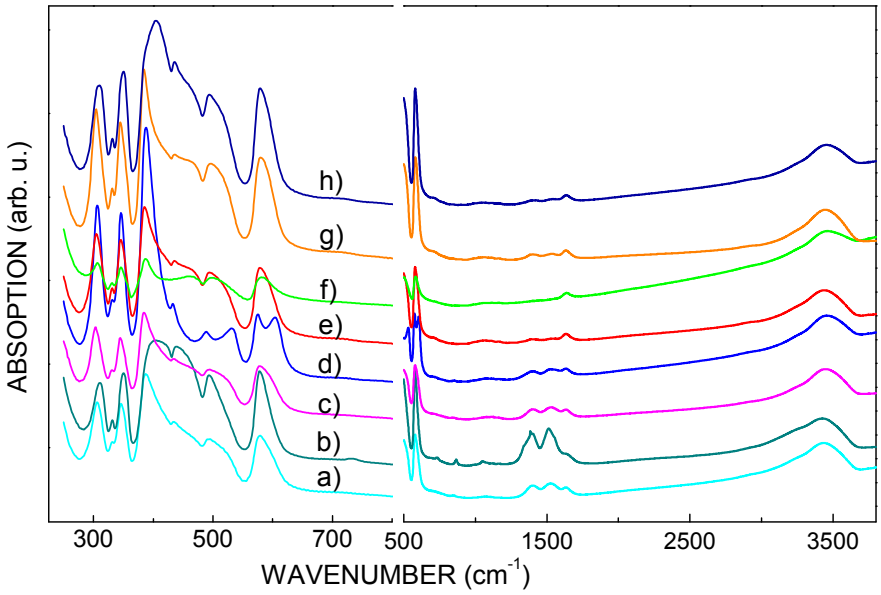

Figure ESI-4. Room temperature FT-IR spectra of nanocrystalline $Lu_{1.99}Tm_{0.01}O_3$ prepared from different synthesis conditions: a) **S**-NIT1-A, b) **S**-NIT1-B, c) **S**-NIT2-A, d) **S**-NIT2-B, e) **S**-CHL1-A, f) **S**-CHL1-B, g) **S**-CHL2-A, h) **S**-CHL2-B.

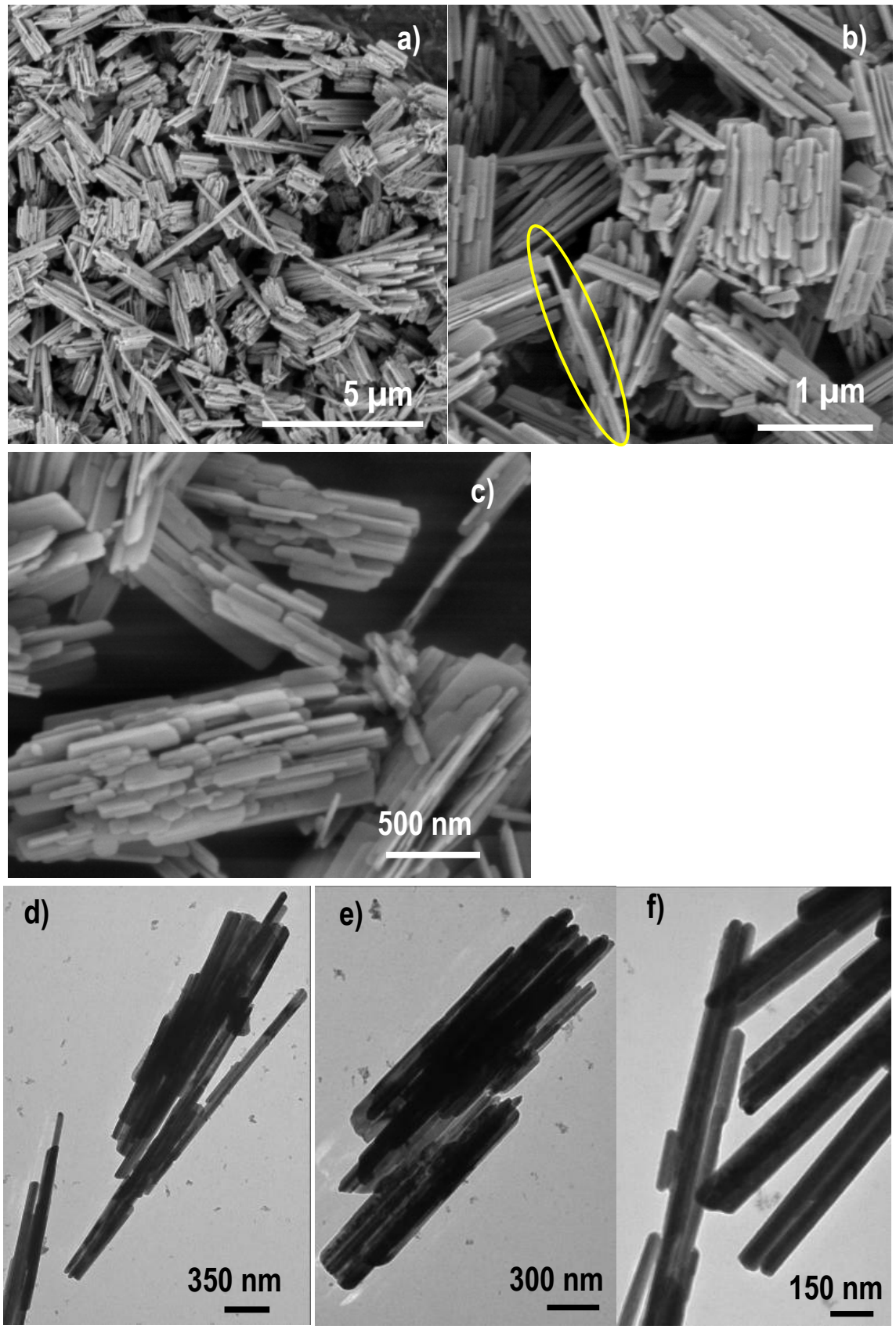

Figure ESI-5. a) and b) FE-SEM images of hydrothermal **P**-NIT1-A, showing highlighted in yellow an assembly of nanorods, c) FE-SEM view of **P**-NIT1-B. d), e) and f) TEM images of alongside assembled nanorods in **P**-NIT1-A, also showing nanoparticles.

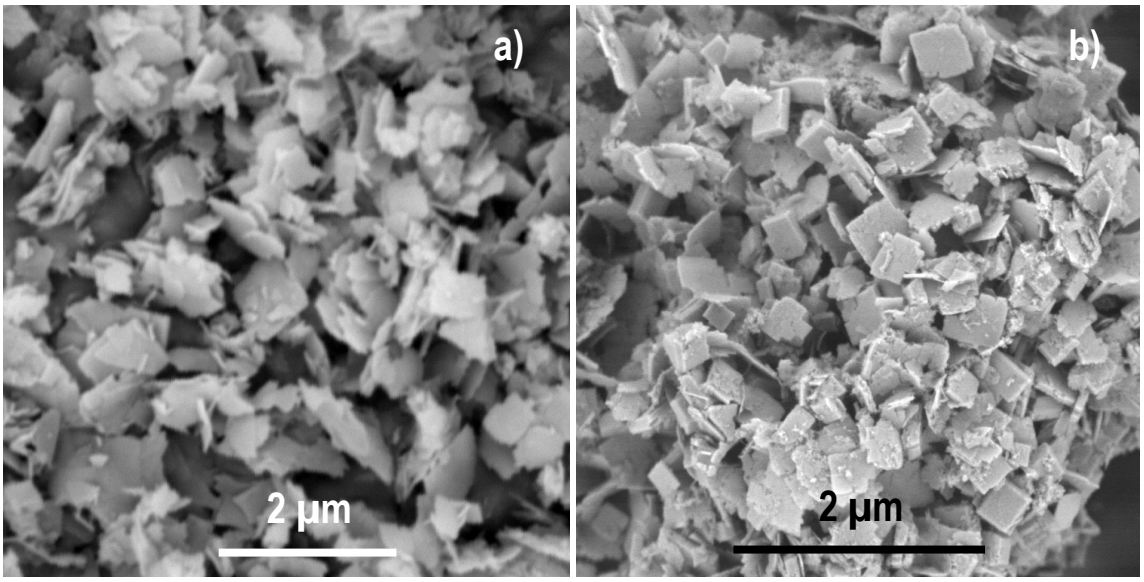

Figure ESI-6. FE-SEM images of hydrothermal nitrate-derived precursors from alkaline media with pH 12, **P**-NIT2, showing square nanosheets a) by using NH_4OH, **P**-NIT2-A, b) by using KOH, **P**-NIT2-B.

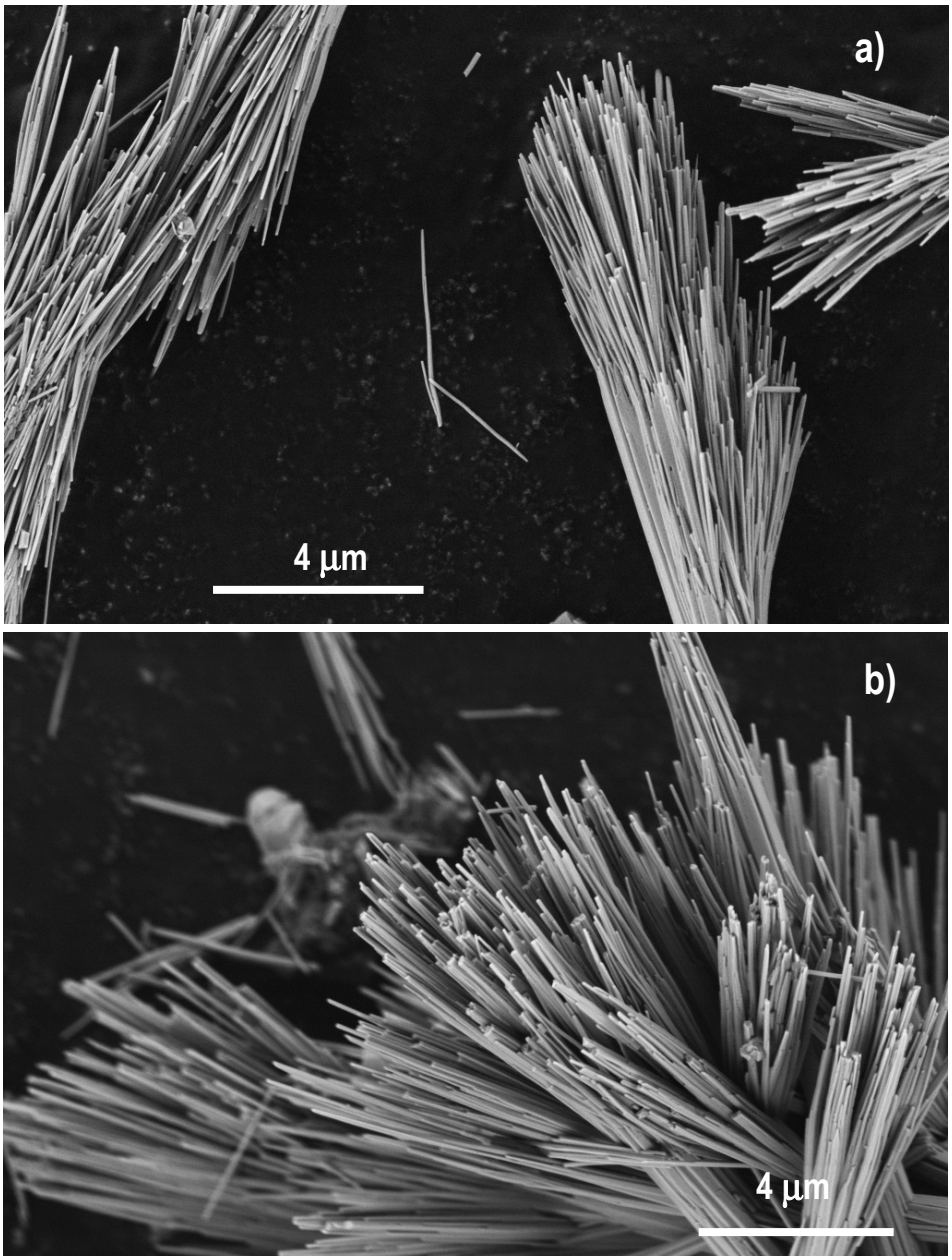

Figure ESI-7. FE-SEM images of hydrothermal chloride-derived precursors from alkaline media with pH 7 by using NH_4OH **P**-CHL1-A, showing characteristic sheaves of nanorods of ~90 nm of diameter.

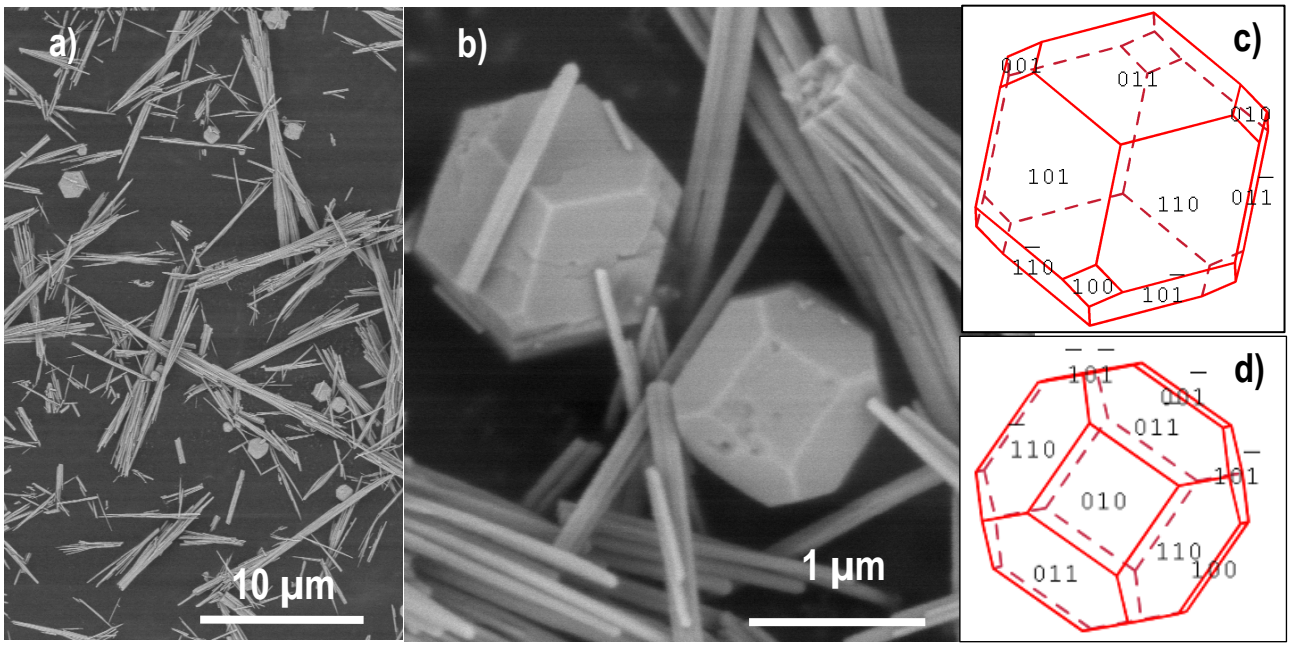

Figure ESI-8. FE-SEM images of hydrothermal precursors prepared from chloride-reagents and pH 7 by using KOH, **P**-CHL1-B: a) and b) Panoramic and detailed views showing bundles of nanorods of ~20 µm of length along with microsized polyhedra, respectively. c) and d) Simulated shape of Tm-Lu_2O_3 grown crystals with {110} and {100} facets.

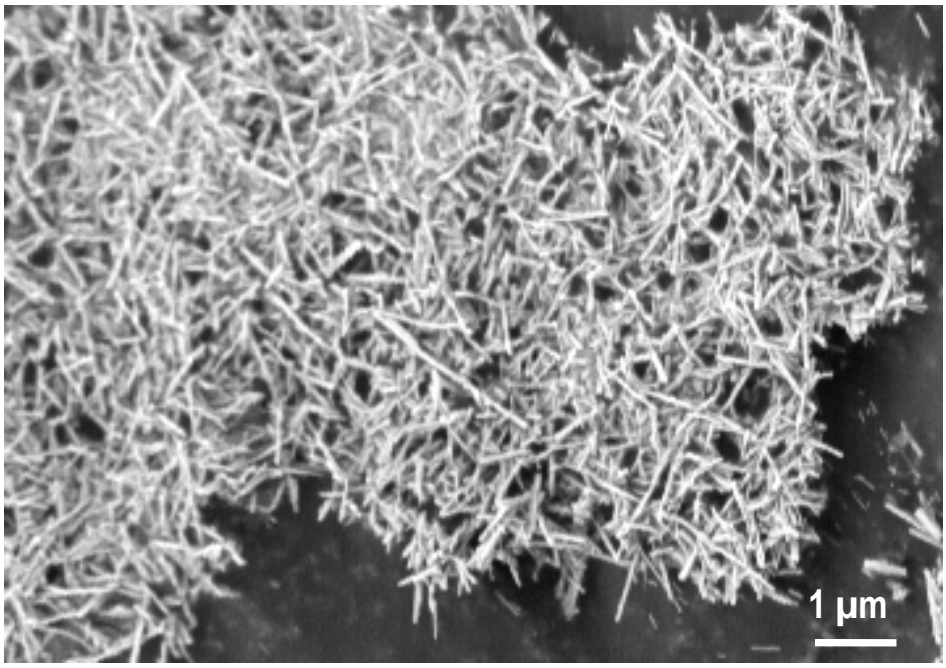

Figure ESI-9. FE-SEM image of nanowires of the hydrothermal precursor prepared with chloride-reagents and pH 12 by using NH_4OH, **P**-CHL2-A.

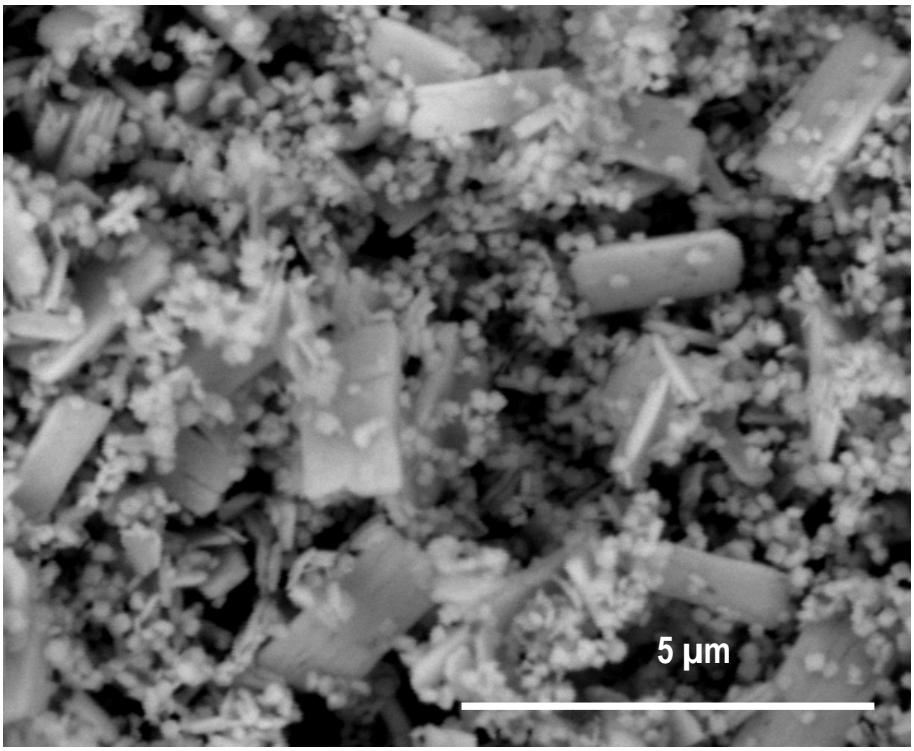

Figure ESI-10. FE-SEM image of microsized tablets and square, hexagon and rod-like nanoparticles of the hydrothermal precursor prepared with chloride-reagents at pH 12 by using KOH, **P**-CHL2-B

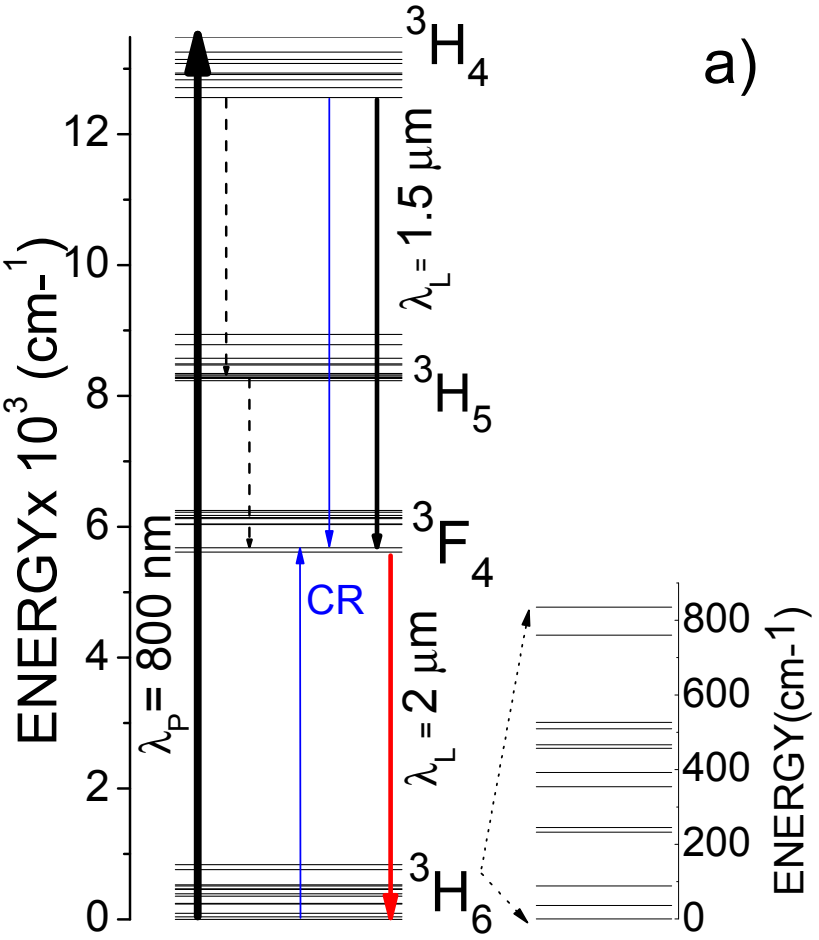

Figure ESI-11. a) Scheme of energy levels of Tm^{3+} in Lu_2O_3, showing relevant pumping and de-excitation paths involved in laser emissions operating at ~2 µm ($^3F_4 \rightarrow {}^3H_6$ transition) and ~1.5 µm ($^3H_4 \rightarrow {}^3F_4$ transition). Tm^{3+} ions can be efficiently excited around 800 nm through the ground state optical absorption of the $^3H_4$ multiplet. The laser multiplet $^3F_4$ is populated either by intraionic electron relaxation or by a cooperative cross-relaxation (CR) process that occurs through the interaction of two neighboring Tm^{3+} ions, $^3H_4 + {}^3H_6 \rightarrow 2\times{}^3F_4$. This laser channel can be directly and efficiently pumped with commercially available powerful semiconductor AlGaAs laser diodes around 800 nm, with little heat transfer to the crystal host. Note that the lower level for the 1.5 µm transition is the $^3F_4$ multiplet, which is at the same time the upper level of the 2 µm emission.

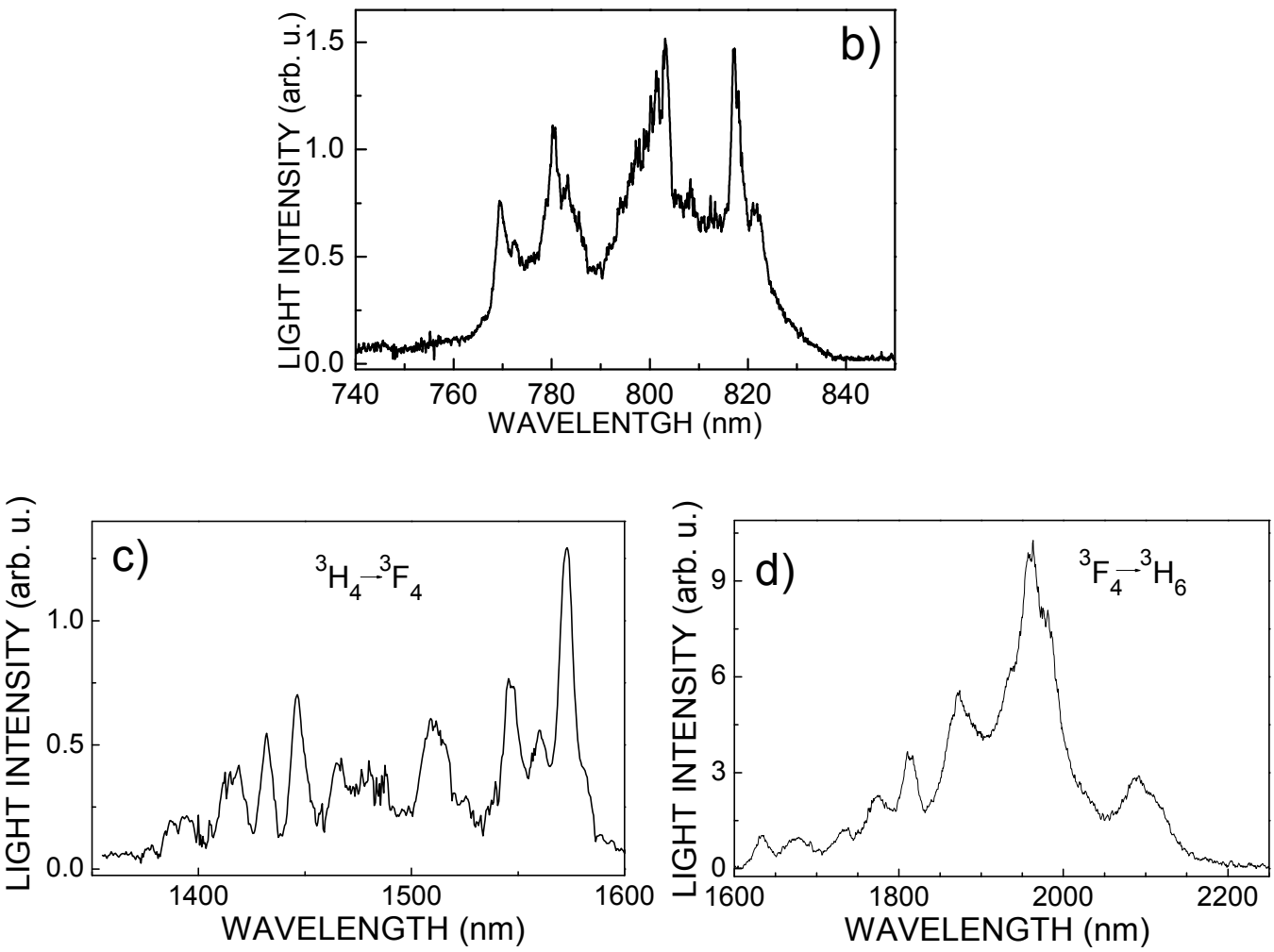

Figure ESI-11 b) 300 K excitation spectrum (λ_{EMI}=1962 nm) of the $^3H_4$ multiplet of S-CHL1-A $Lu_{1.99}$ $Tm_{0.01}O_3$. 300 K photoluminescence (λ_{EXC}=802 nm) spectra of S-CHL1-A $Lu_{1.99}Tm_{0.01}O_3$: c) $^3H_4 \rightarrow {}^3F_4$ and d) $^3F_4 \rightarrow {}^3H_6$.